Carbon 150 (2019) 268–274

Contents lists available at ScienceDirect

Carbon

journal homepage: www.elsevier.com/locate/carbon

# Enhancing the strength, toughness, and electrical conductivity of twist-spun carbon nanotube yarns by π bridging

Xiumin Liang [a, 1], Yuan Gao [a, 1], Jianli Duan [a, 1], Zunfeng Liu [b], Shaoli Fang [c], Ray H. Baughman [c], Lei Jiang [a], Qunfeng Cheng [a, *]

[a] Key Laboratory of Bio-inspired Smart Interfacial Science and Technology of Ministry of Education, School of Chemistry, Beijing Advanced Innovation Center for Biomedical Engineering, Beihang University, Beijing, 100191, PR China
[b] State Key Laboratory of Medicinal Chemical Biology, Key Laboratory of Functional Polymer Materials, Ministry of Education, College of Pharmacy, Nankai University, Tianjin, China
[c] The Alan G. MacDiarmid NanoTech Institute, University of Texas at Dallas Richardson, TX, 75080, USA

ARTICLE INFO

*Article history:*
Received 5 December 2018
Received in revised form
3 May 2019
Accepted 8 May 2019
Available online 10 May 2019

*Keywords:*
Carbon nanotube
Yarn
π bridging
Mechanical properties

ABSTRACT

The weak interfacial interactions between carbon nanotube (CNT) always results in low stress load transfer efficiency in CNT yarns, herein we fabricated strong, highly conducting CNT yarns at room temperature using molecules having aromatic end groups, π bridging neighboring CNTs. The resulting CNT yarns have high tensile strength with 1697 ± 24 MPa, toughness with 18.6 ± 1.6 MJ/m$^3$, and electrical conductivity with 656.2 S/cm, which are 3.9, 2.5, and 3.5 times, respectively, as high as that of the neat CNT yarn. The specific tensile strength of the resulting CNT yarn is higher than that for previously reported CNT yarns fabricated at room temperature, even that for some CNT yarns fabricated using corossive environments or extreme temperature. This π bridging strategy provides a promising avenue for fabricating high performance CNT yarns under ambient conditions.



## 1. Introduction

Carbon nanotubes (CNTs) stand out as an ideal one-dimensional nanomaterial, with a tensile strength of about 100 GPa and a Young's modulus of about 1 TPa [1]. Superaligned CNT forests provide a useful platform for assembling CNT yarns through a solid spinning process [2–4]. However, the resulting CNT yarns show much lower mechanical properties than individual CNT, due to weak interfacial interactions between individual CNT and non-uniform stresses [5,6]. Many approaches have been developed to improve the interfacial strength in the CNTs [7–11]. For example, Boncel et al. [12] utilized ultraviolet-radiation-reacted 1,5-hexadiene (HDE) to enhance interfacial interactions. Liu et al. [13] introduced hydrogen bonding between individual CNTs by infiltrating polyvinyl alcohol (PVA), resulting in high PVA content up to about 19 wt%. Ryu et al. [14] obtained strong superaligned CNT yarn through infiltrating 8 wt% of adhesive poly (ethylenimine) catechol (PEI-C). Using thermal annealing, π-π interactions were introduced into PEI-C/CNT yarns, resulting in a tensile strength of up to 2200 MPa. Recently, Ryu et al. [15] infiltrated superaligned CNT yarns with dopamine (DA) solution, thereby introducing oxidatively polymerized dopamine (PDA) between individual CNTs. After annealing at 1050 °C, the CNT-wrapped PDA partially pyrolyzed, thereby interconnecting the superaligned CNTs through π-π interactions. The resulting superaligned CNT yarns had a tensile strength of about 4 GPa. Im et al. [16] demonstrated high performance CNT fiber with a specific strength of 1.12 N/tex through crosslinking CNT fiber via 1,5-pentanediol. Lu et al. [17] introduced covalent cross-linking through coating CNT with poly (styrene-r-4-vinylbenzylcyclobutene) (PS-VBCB) and thermal annealing at 250 °C. The resulting CNT yarns having 7 wt% PS-VBCB had a tensile strength of only 260 MPa. Similarly, Park et al. [18] assembled covalently cross-linked CNTs by using aryl radical coupling reactions of poly (p-iodostyrene) (PIS), which resulted from thermal annealing at 350 °C. However, the used PIS content was as high as 50 wt%, and the specific tensile strengh of the PIS/CNTs yarns was only 1.4 N/tex. They further studied the effect of the degree of cross-linking, length of cross-linkers, and CNT diameter on mechanical properties of resultant CNT fibers [19]. Although the mechanical properties of CNT yarns have been improved, harsh conditions,

* Corresponding author.
*E-mail address:* cheng@buaa.edu.cn (Q. Cheng).
[1] These three authors contributed equally to this work.

https://doi.org/10.1016/j.carbon.2019.05.023
0008-6223/

such as high temperature annealing, were needed. Consequently, it remains challenging to realize attractive mechanical properties for the CNT yarns without using harsh conditions.

Herein, we fabricated strong CNT yarns using π bridging between CNTs by pyrene-group-terminated PSE-AP molecules, which are produced by the reaction of 1-pyrenebutyric acid N-hydroxysuccinimide ester (PSE) and 1-aminopyrene (AP), as shown in Fig. S1. With reference to previous works, we selected specific bridging agents PSE and AP. Katz et al. [20] reported that PSE can be used as an anchor group for chemisorption on the pyrolytic graphite surface and the chemically active NH group of the protein can furthur react with PSE. AP is a typical molecule which can form PSE-AP with PSE through this reaction. It is well known that AP can strongly bind to the surface of CNTs [21]. We have reported graphene oxide (GO) fiber with improved mechanical and electrical properties *via* the synergistic effect of ionic bond and π-π conjugated interaction from PSE-AP [22]. However, there are still some differences, such as the surface functional structure, assembling approach, etc. The mechanical properties of the resulting CNT yarns are dramatically increased by introducing at room temperature a low concentration of PSE-AP molecules. The tensile strength, specific tensile strength, and toughness of the resulting CNT yarns reach 1697 MPa, 2.8 N/tex, and 18.6 MJ/m$^3$, respectively. Additionally, because the π-π conjugated molecules increase connections between CNTs in CNT yarn, the PSE-AP enhanced CNT yarns provided an increased electrical conductivity of 656 S/cm.

## 2. Experimental

### 2.1. Materials

The CNT forests were synthesized by a chemical vapor deposition (CVD) of acetylene gas. 1-Pyrenebutyric acid N-hydroxysuccinimide ester (PSE) and 1-Aminopyrene (AP) were purchased from Sigma-Aldrich. N, N-Dimethylformamide (DMF) was obtained from Beijing Chemical Factory. All the reagents were used without further purification.

### 2.2. Fabrication of twist-spun CNT yarns and introduction of PSE-AP cross-linker in the yarns

A CNT sheet ribbon with a fixed width was drawn from a CNT forest as it was twist spun to make a yarn having a bias angle of 18–20°, and a diameter of ~15 μm. The complete fabrication process is described in detail in the main text.

### 2.3. Characterization

The mechanical properties of 3-cm-long CNT yarns were characterized using a Shimadzu AGS-X Tester, using a strain rate of 0.4 mm/min. All measurements were conducted at room temperature. The diameters of all samples were measured using scanning electron microscopy (SEM) micrographs. The Young's modulus of all samples was determined from the slope of the linear region of the stress-strain curves. The toughness was calculated from the area under the stress-strain curves. Usually, the 10–15 specimens of each type CNT yarn sample are used for tensile testing, and 3–5 well repeatable specimens are selected for calculating the average mechanical properties of each sample. The specific strength was calculated by dividing the tensile load at failure by the linear density of the yarn. SEM images were recorded by a Hitachi S-4800 at 11.5 kV after sputtering a thin Pt/Au coating onto the samples. The cross sectional SEM images of CNT yarn and cross-linked CNT yarn (CNTs Yarn-III) shown in Fig. S7 were obtained by focused ion beam (FIB) and SEM on a FEI Helios NanoLab 600i. TGA from 30 to 800 °C was performed under nitrogen on a TG/DTA6300, NSK using a temperature scan rate of 10 °C/minute. The calculation of the weight fraction of PSE-AP molecules in the cross-linked CNT yarn (CNTs Yarn-III) is shown in the Supporting Information. Raman spectroscopy measurements were taken on a LabRAM HR800 (Horiba JobinYvon) with an excitation energy of 1.96 eV (633 nm). XPS measurements were carried out in an ESCALab220i-XL (Thermo Scientific) using a monochromatic Al-Ka X-ray source. The electrical conductivities were measured using a standard two-probe method and a source meter (Agilent E4980A). The two ends of yarns were fixed by silver paste in order to decrease the contact resistance with the probes. FTIR spectra was conducted using a Thermo Nicolet Nexus-470 FTIR instrument in the attenuated total reflection mode (ATR).

## 3. Results and discussion

The fabrication process for making these CNT yarns is illustrated in Fig. 1a. A forest of vertically superaligned CNTs was attached to a motor, which rapidly rotated the superaligned CNT forest as a CNT sheet was drawn from the forest, thereby producing a twisted CNT yarn. Using previous report of the twist angle that optimizes strength [6,23], the twist angle of CNT yarns was set at about 18–20°. N, N-dimethylformamide (DMF) solvent was sprayed on the surface of the CNT yarn to densify the yarn and then the CNTs-DMF yarn was obtained, followed by the post-treatments. Firstly, the densified CNTs-DMF yarn was immersed into a solution of PSE in DMF to enable absorption of PSE molecules on the CNT surfaces within the yarn. Secondly, after drying, the CNTs-PSE yarn was immersed into an solution of AP in DMF that has the same molarity as the PSE/DMF solution. After drying, the yarn was immersed into DMF in order to remove unreactive PSE and AP. Finally, after drying to remove DMF solvent, the CNTs-PSE-AP yarn was collected on a spindle.

The used 200-μm-high CNT forest of about 10-nm-diameter multiwalled carbon nanotubes (MWNTs) is pictured in Fig. 1b and 1c shows a magnified view of a superaligned CNT forest sidewall. The structural transformation during sheet draw and sheet twist processes to make a twisted yarn is shown in Fig. 1d. The produced CNTs-PSE-AP yarn is pictured in Fig. 1e. The yarn has a twist angle (the angle between the CNT orientation direction and fiber length direction) of about 18.5° and a diameter of about 15 μm. Fig. 1f illustrates the interfacial interaction between CNTs and PSE-AP in a CNTs-PSE-AP yarn. To optimize the mechanical properties of CNTs-PSE-AP yarns, the content of π–π conjugated molecules was tailored. The CNT yarns were immersed into solution with five different molarities of PSE and AP (18 mmol/L, 48 mmol/L, 72 mmol/L, 90 mmol/L, and 108 mmol/L) for 2 h, and the resulting CNTs-PSE-AP yarns are designated as: CNTs Yarn-I, CNTs Yarn-II, CNTs Yarn-III, CNTs Yarn-IV, and CNTs Yarn-V, respectively, which are listed in Table S1. The immersion time was optimized by trying 5 different times, the mechanical properties are listed in Table S2.

Fourier transform infrared (FTIR) spectra was used to confirm the reaction between PSE and AP molecules (Fig. 2a). The characteristic peak at 1540 cm$^{-1}$ for a CNTs-PSE-AP yarn corresponds to the bending of the N–H bond in amide group. The stretching mode of C=O bond in amide groups of PSE-AP is observed at 1670 cm$^{-1}$ in the CNTs-PSE-AP yarn. These characteristic peaks indicate that the amide groups were successfully introduced in the CNTs-PSE-AP yarn. The results of X-ray photoelectron spectra (XPS) show the existence of a new peak of 288.2 eV, which is due to C–N sp [3] bond [17], indicating the π–π conjugated molecules were strongly absorbed onto the CNT surface, as shown in Figs. 2b and S2. Raman spectra for the different samples are shown in Fig. 2c, and the relative peak intensity ratios of the D band (~1300 cm$^{-1}$) to the G

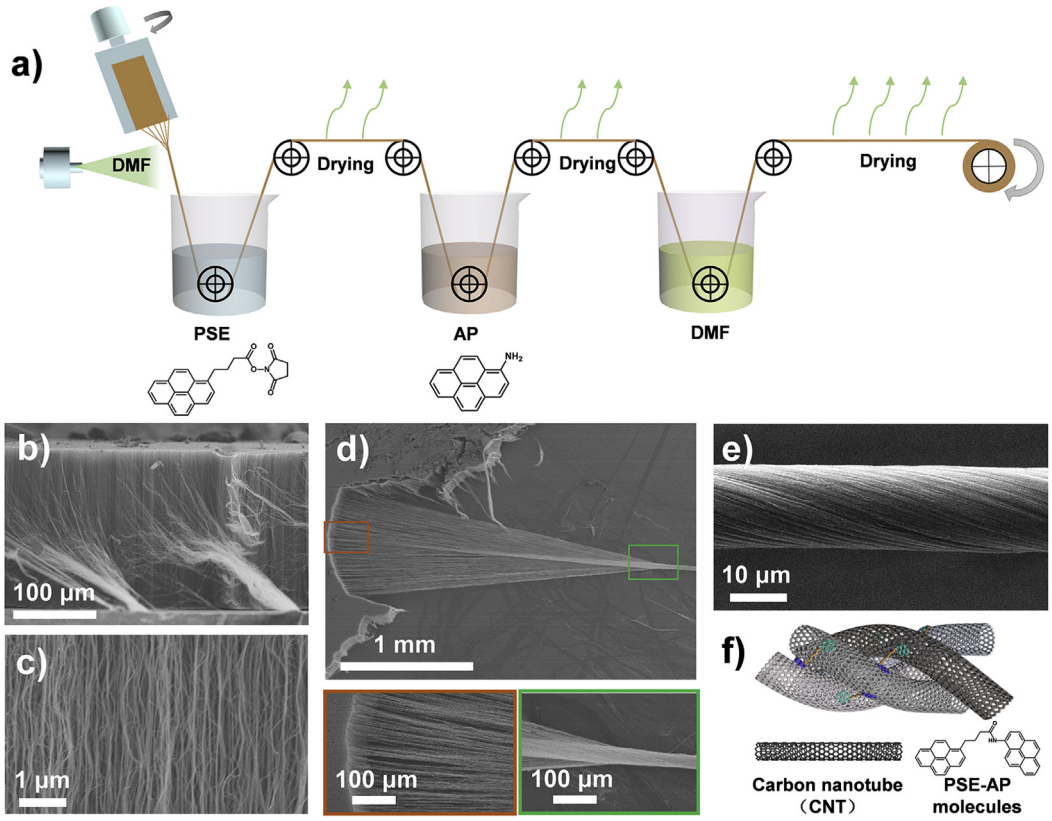


**Fig. 1.** a) Schematic illustration of the fabrication of a CNTs-PSE-AP yarn. b), c) SEM images of a CNT forest grown on a silicon substrate, revealing the alignment of CNT bundles. d) SEM image of a CNT yarn being formed by twist insertion a forest-drawn CNT sheet. e) SEM image of a CNTs-PSE-AP yarn. f) Schematic diagram of the interfacial interactions between CNTs and PSE-AP in the CNTs-PSE-AP yarn.

band (~1590 $cm^{-1}$) are listed in Table S3. The relative peak intensity ratio of the D band to the G band ($I_D/I_G$) increases after functionalization, indicating the introduction of π−π conjugated molecules in CNTs-PSE-AP yarns. Additionally, the CNTs-PSE-AP yarns provide high electrical conductivities, with a maximum of 656.2 S/cm for CNTs Yarn-V, as shown in Fig. 2d. The electrical conductivites for the other CNTs-PSE-AP yarns are listed in Table S4. The electrical conductivities of the CNTs-PSE-AP yarns are significantly higher than that of other CNT yarns, such as CNT-polypyrrole (PPy) yarn [24], poly (3,4-ethylenedioxythiophene) (PEDOT)-MWCNT yarn [25] and CNT-poly (acrylic acid) (PAA) yarn [26]. The improvement of electrical conductivity is attributed to densification [27], and the doping on the CNT [28], respectively. In this work, the π-π conjugated interactions between CNTs and PSE-AP plays a key role in enhancing the electrical conductivity of the resultant CNT yarns.

Representative stress-strain curves of all yarns are shown in Fig. 3a. The tensile strength and toughness of the initial CNT yarn (Curve 1) are 432 ± 20 MPa and 7.4 ± 0.9 $MJ/m^3$. Herein the toughness means the tensile fracture energy, which is calculated by area under tensile stress-strain curves. After densification using DMF solvent, the tensile strength and toughness of the CNTs-DMF yarn (Curve 2) reach 1045 ± 23 MPa and 12.4 ± 0.6 $MJ/m^3$. The CNTs Yarn-III (Curve 3) had a maximum tensile strength of 1697 ± 24 MPa and a toughness of 18.6 ± 1.6 $MJ/m^3$, which are 3.9 and 2.5 times as high as those of precurser CNT yarn. The stress−strain curves of the CNT, CNTs-DMF, and CNTs-PSE-AP yarns are shown in Fig. S3. The pure CNT yarn shows a large elongation at break due to weak interfacial interactions between CNTs. After π-π conjugated cross-linking, the relative slip between CNTs is limited, resulting in lower elongation at break. Meanwhile, the stress transfer efficiency is dramatically improved, enhancing the tensile strength and modulus. Fig. 3b, c and 3d show the tensile strength, toughness, and modulus of CNT yarn, CNTs-DMF yarn and CNTs-PSE-AP yarns having different contents of PSE-AP molecules, and the numerical values are listed in Table S5. With increasing PSE-AP content, the mechanical properties of the CNTs-PSE-AP yarns first increase, reaching a maximum in CNTs Yarn-III, and then decrease. The content of PSE-AP in CNTs Yarn-III is about 1.6 wt%, using thermogravimetric analysis, as shown in Fig. S4. The PSE-AP contents for all CNTs-PSE-AP yarns are shown in Table S6. While the content of PSE-AP in the yarns is so low, effective cross-linking between CNTs by the PSE-AP can be achieved, facilitating load transfer between CNTs. However, when the content of PSE-AP molecules further increases, as for CNTs Yarn-IV and CNTs Yarn-V, the mechanical properties decrease. This decrease might because cross-linking molecules are wasted in stacking between themselves instead of cross-linking CNT bundles. Excessive cross-linking molecules present between the CNT bundles may cause defects inside the yarns, reduce the friction between the CNTs, and cannot produce effective cross-linking, so it cannot contribute to the improvement of yarns mechanical properties [29,30].

A typical morphology of the fractured surface of CNTs Yarn-III is shown in Fig. 3e, which shows that CNT bundles are pulled from the yarn during fracture. A crack propagation model, shown in Fig. 3f, is proposed to explain the fracture mechanism of the CNTs-PSE-AP yarns. In the first stage, when the CNTs-PSE-AP yarn is subjected to the stress, the load transfer efficiency increases as a result of relative slip of CNT bundles and real plastic deformation of

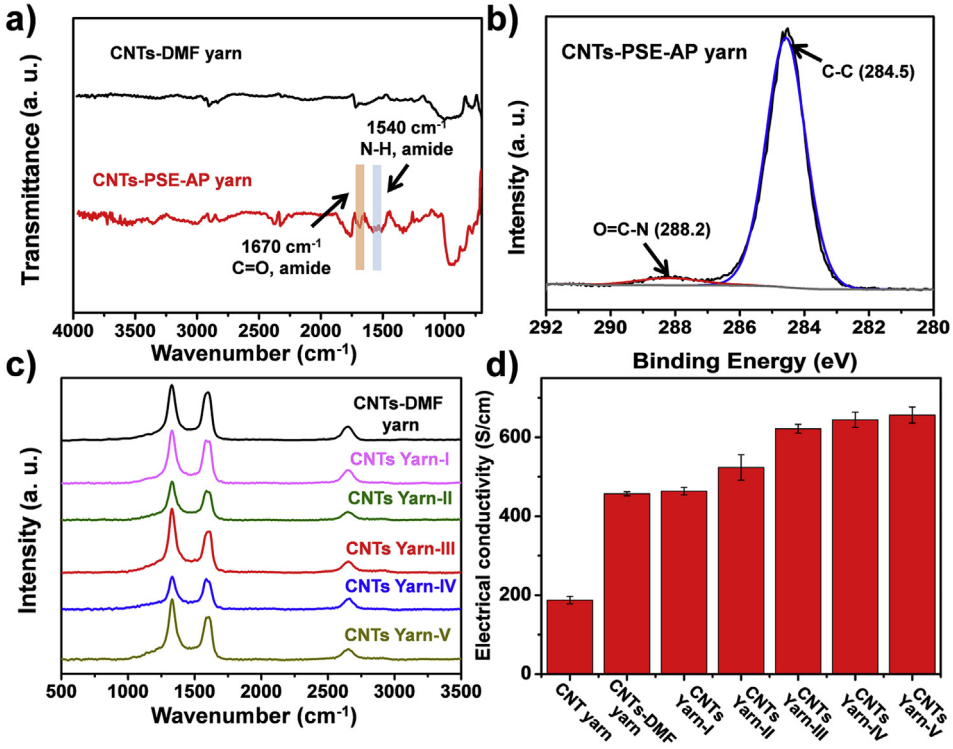


**Fig. 2.** a) FTIR spectra of a CNTs-DMF yarn and a CNTs-PSE-AP yarn, showing that reaction occurred between PSE and AP molecules. b) XPS spectrum of a CNTs-PSE-AP yarn. The peak at 288.2 eV reflects C–N sp [3] bond, indicating that reaction has occurred to produce PSE-AP and that this molecule is strongly absorbed on the CNT surfaces and cannot be washed away by the solvent. c) Raman spectra of CNTs-DMF yarn, CNTs Yarn-I, CNTs Yarn-II, CNTs Yarn-III, CNTs Yarn-IV, and CNTs Yarn-V. The intensity ratio $I_D/I_G$ of CNTs-DMF is 1.17, and the $I_D/I_G$ of CNTs-PSE-AP yarns increases with rising content of PSE-AP molecules in the yarns. d) Electrical conductivity of CNT yarn, CNTs-DMF yarn, and CNTs-PSE-AP yarns.

individual nanotubes [31]. When an external load acts on the yarns to cause the CNTs to slip between each other, the PSE-AP molecules are stretched along the direction of stretching. And as the tensile load increases, due to the non-covalent π-π interaction inherent characteristic, the pyrene group on the PSE-AP slips relative to the CNT. At this stage, load transfer effeciency is promoted by π-π interaction to avoid local stress concentration [24]. Finally, the CNTs-PSE-AP yarn breaks with increasing tensile load, resulting in further rupture of π-π cross-linking and accompanying energy dissipation as the CNT bundles are pulled from the yarn under high tensile stress. For comparison, the fracture morphologies of a neat CNT yarn and the CNTs-PSE-AP yarns are shown in Fig. S6. When the CNT-based yarn is subjected to tensile load, there will be relative slip between the internal CNTs. Therefore, the fracture morphology can clearly show that the CNTs are pulled out. The fracture morphology of CNT yarns before cross-linking is mainly pull-out of single carbon nanotube. After cross-linking, it can be clearly seen that the carbon nanotubes are connected to each other, so that the carbon nanotubes are pulled out in a bundle-like manner. And the cross-linking is obviously effective in improving the stress transmission efficiency, resulting in high mechanical properties of the CNT yarns. In addition, the cross-sectional morphology of the CNT yarns shown in Fig. S7 indicates that the compactness of the CNT yarns after cross-linking is improved, and the internal pores are reduced. The surface morphologies of CNT yarn and the CNTs-PSE-AP yarns are provided in Fig. S5, showing the surface of cross-linked CNT Yarns is flatter, and proving that the introduction of the cross-linking molecule by immersion does not damage the CNT yarn's structure, and the twist angle of CNT yarns does not change significantly.

The specific strength of the resulting CNTs-PSE-AP yarns is calculated, based on the tensile load (cN or N) and yarn linear density (tex), which is the standard method adopted in the textile industry [32]. The specific strength and toughness of the optimized CNTs-PSE-AP (2.8 N/tex and 30.5 J/g) is compared in Fig. 4a with that of other CNT yarns and other fibers. As shown in this figure, the present CNTs-PSE-AP yarns provide a combination of specific strength and specific toughness that is attractive relative to the properties of the following: twist-spun CNT yarn [3], incandescent tension annealed (ITAP) CNT yarn [33], HDE-UV-CNT fiber [12], SACNT (superaligned CNT)-PVA yarn [13], pyrolized-PDA-CNT yarn [15], UHMW-PE (ultrahigh molecular weight PE fibers) [34], thermally treated nylon fibers [35], spider silk [36,37], in-situ CVD-grown double-walled nanotube (DWNT) yarns [38], polymer/DWNT yarns [39], and glass fibers [39]. Harsh conditions, such as high temperatures or high pressures, can result in strong cross-linking between CNTs, but the toughnesses of resulting CNT yarns are usually low.

It is especially important that the present CNT yarns are assembled at room temperature using a very simple process that does not involve expensive or corrosive chemicals. The π–π interactions do not damage the sp [2] carbon structures of CNTs, which is the case for many other processes. To use the PSE-AP inter-nanotube cross-linkers improves the efficiency of load transfer between CNTs, resulting in attractive mechanical properties. The mechanical properties of other CNT yarns, other fibers, and the yarn presently obtained (CNTs Yarn-III) are listed in Table S7. The electrical conductivity of the PSE-AP cross-linked CNTs Yarn-V (656 S/cm) is 3.5 times that for the precurser CNT yarn, which is attributed to the following two reasons: First, the crosslinking of PSE-AP helps

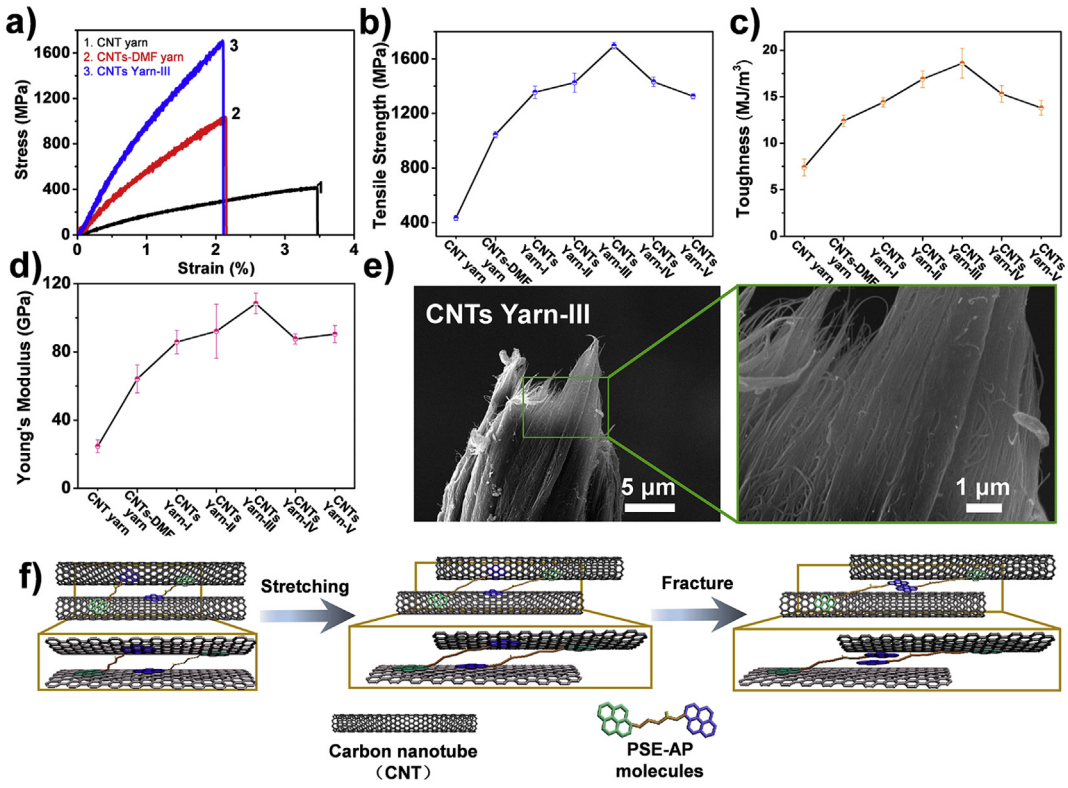


**Fig. 3.** a) Typical stress-strain curves of CNT yarn (Curve 1), CNTs-DMF yarn (Curve 2) and CNTs Yarn-III (Curve 3). The tensile strength b), toughness c) and modulus d) of CNT yarn, CNTs-DMF yarn and CNTs-PSE-AP yarn having different PSE-AP content. e) SEM images of the fracture morphology of CNTs Yarn-III after tensile rupture at different magnifications. f) The proposed fracture mechanism of the PSE-AP cross-linked CNT yarn during stretching.

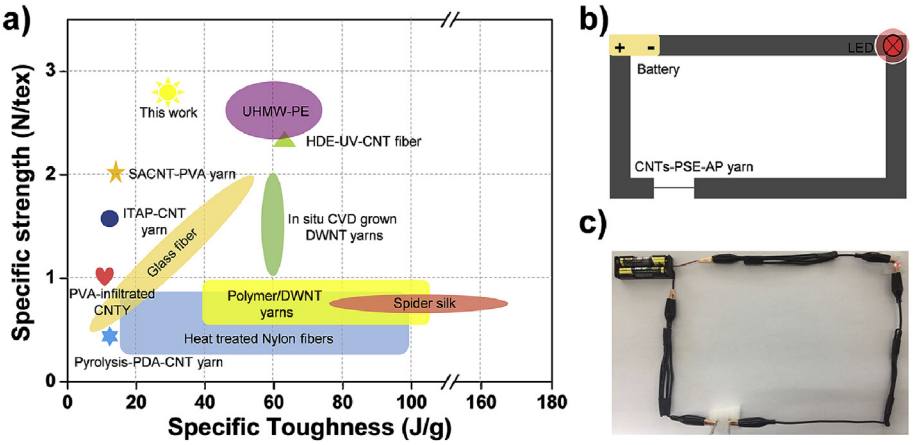


**Fig. 4.** a) Comparison of the specific strength and specific toughness of CNTs-PSE-AP yarns in this work, along with that of other CNT yarns and other fibers. b) Schematic of a circuit in which CNTs-PSE-AP yarns are used as wiring. c) Photograph CNTs-PSE-AP yarn serving as wiring to conduct current to light a red LED bulb.

to increase the compactness of CNT yarn. The cross-sectional morphology of the PSE-AP cross-linked CNT yarn obtained by focused ion beam (FIB) shows that the porosity in the fibers is significantly reduced after PSE-AP crosslinking (Fig. S7). The internal structure is more compact, which is more conducive to the transmission of electrons inside the yarns. Second, a strong amide bond is formed between the PSE and the AP molecules, and the benzene ring at both ends of the PSE-AP molecule forms a π-π conjugate with CNT. The dipole-dipole interaction formed in the π-π interaction is beneficial to improve the electron transport efficiency [24], thereby resulting in enhancement of the electrical conductivity of the CNT yarns. Even if there are PSE-AP molecules stacking between themselves instead of cross-linking CNT bundles, they may form an electron transport path due to π-π conjugation, so that conductivity is not reduced. It can be seen from the conductivity data that the conductivity increase of CNTs Yarn IV and CNTs Yarn V is significantly lower than that of the yarns with low PSE-AP addition, which also indicates that too much cross-linking molecules may don't form very effective connection between CNTs. The CNTs-PSE-AP yarns can be used as wiring to connect a red

LED light to a power source, as shown in Fig. 4b and c.

The interfacial interaction between PSE-AP and CNT is mainly due to the fact that the aromatic structure forms a π-π conjugate with the aromatic structure of the CNT. Therefore, other molecules with aromatic structure at both ends also can be used for cross-linking CNTs. A series of works have been carried out to discuss the adsorption and conjugation of different aromatic structures on the surface of CNTs [40–42]. The aromatic structure molecules with different aromatic ring numbers and sizes may have different effect on tensile strengths of CNTs yarn. At present, we have not tried the π-π conjugated cross-linking of other molecules on CNTs yarn, but demonstrated AP and another reactive π-crosslinking molecule for improving the mechanical properties of the graphene film [43].

## 4. Conclusion

In summary, we demonstrated that strong, tough, highly conducting CNT yarns can be fabricated at room temperature by an inexpensive process that does not use corrosive chemicals. This process uses a low concentration of a non-covalent π–π cross-linker to strengthen inter-nanotube interactions. The obtained tensile strength of $1697 \pm 24$ MPa, toughness of $18.6 \pm 1.6$ MJ/m$^3$ and electrical conductivity of $656.2 \pm 20.5$ S/cm are 3.9, 2.5 and 3.5 times, respectively, as high as that of the precurser CNT yarn. The observed specific strength was as high as 2.8 N/tex. The π bridging strategy is very feasible and without any harsh conditions, providing an insightful approach for constructing high performance CNT yarns in the future.

## Acknowledgement

We would like to thank Jingsong Peng, Weixin Huang, Can Cao, Yifei Luo, Teng Ke, Huiwen Tian, and Yuanyuan Zhang for carefully checking the manuscript. We would like to thank the Center for Bioenergy Innovation, Institute of Biophysics, Chinese Academy of Science for our FIB Microscopy and we would be grateful to Xing Jia for her help of taking Electron Microscopy images. This work was supported by the Excellent Young Scientist Foundation of NSFC (51522301), the National Natural Science Foundation of China (21875010, 21273017, 51103004), the Program for New Century Excellent Talents in University (NCET-12-0034), the Fok Ying Tong Education Foundation (141045), the 111 Project (B14009), the Aeronautical Science Foundation of China (20145251035, 2015ZF21009), State Key Laboratory of Organic–Inorganic Composites, Beijing University of Chemical Technology (oic-201701007), the State Key Laboratory for Modification of Chemical Fibers and Polymer Materials, Donghua University (LK1710), the Fundamental Research Funds for the Central Universities (YWF-16-BJ-J-09, YWF-17-BJ-J-33, YWF-18-BJ-J-13) and the Academic Excellence Foundation of BUAA (20170666) for Ph.D. Students. Funding support in United States was from NSF Award 1636306 and a Robert A. Welch Foundation grant (AT-0029).

## Appendix A. Supplementary data

Supplementary data to this article can be found online at https://doi.org/10.1016/j.carbon.2019.05.023.

## References

[1] B. Peng, M. Locascio, P. Zapol, S.Y. Li, S.L. Mielke, G.C. Schatz, et al., Measurements of near-ultimate strength for multiwalled carbon nanotubes and irradiation-induced crosslinking improvements, Nat. Nanotechnol. 3 (2008) 626–631.
[2] K.L. Jiang, Q.Q. Li, S.S. Fan, Spinning continuous carbon nanotube yarns, Nature 419 (2002) 801.
[3] M. Zhang, K.R. Atkinson, R.H. Baughman, Multifunctional carbon nanotube yarns by downsizing an ancient technology, Science 306 (2004) 1358–1361.
[4] M. Zhang, S.L. Fang, A.A. Zakhidov, S.B. Lee, A.E. Aliev, C.D. Williams, et al., Strong, transparent, multifunctional, carbon nanotube sheets, Science 309 (2005) 1215–1219.
[5] X. Zhang, K. Jiang, C. Feng, P. Liu, L. Zhang, J. Kong, et al., Spinning and processing continuous yarns from 4-inch wafer scale super-aligned carbon nanotube arrays, Adv. Mater. 18 (2006) 1505–1510.
[6] W. Ma, L. Liu, R. Yang, T. Zhang, Z. Zhang, L. Song, et al., Monitoring a micromechanical process in macroscale carbon nanotube films and fibers, Adv. Mater. 21 (2009) 603–608.
[7] W.Y. Li, J.N. Zhao, Y. Xue, X.Q. Ren, X.H. Zhang, Q.W. Li, Merge multiple carbon nanotube fibers into a robust yarn, Carbon 145 (2019) 266–272.
[8] X.Y. Lu, N. Hiremath, K.L. Hong, M.C. Evora, V.H. Ranson, A.K. Naskar, G.S. Bhat, N.G. Kang, J.W. Mays, Improving mechanical properties of carbon nanotube fibers through simultaneous solid-state cycloaddition and crosslinking, Nanotechnology 28 (2017) 145603.
[9] O.K. Park, H.K. Choi, H.B. Jeong, Y.S. Jung, J.S. Yu, J.K. Lee, J.Y. Hwang, S.M. Kim, Y.J. Jeong, C.R. Park, M.B. Endo, B.C. Ku, High-modulus and strength carbon nanotube fibers using molecular cross-linking, Carbon 118 (2017) 413–421.
[10] J.N. Zhao, Q.S. Li, B. Gao, X.H. Wang, J.Y. Zou, S. Cong, X.H. Zhang, Z.J. Pan, Q.W. Li, Vibration-assisted infiltration of nano-compounds to strengthen and functionalize carbon nanotube fibers, Carbon 101 (2016) 114–119.
[11] D.M. Mulvihill, N.P. O'Brien, W.A. Curtin, M.A. McCarthy, Potential routes to stronger carbon nanotube fibres via carbon ion irradiation and deposition, Carbon 96 (2016) 1138–1156.
[12] S. Boncel, R.M. Sundaram, A.H. Windle, K.K.K. Koziol, Enhancement of the mechanical properties of directly spun cnt fibers by chemical treatment, ACS Nano 5 (2011) 9339–9344.
[13] K. Liu, Y.H. Sun, X.Y. Lin, R.F. Zhou, J.P. Wang, S.S. Fan, et al., Scratch-resistant, highly conductive, and high-strength carbon nanotube-based composite yarns, ACS Nano 4 (2010) 5827–5834.
[14] S. Ryu, Y. Lee, J.W. Hwang, S. Hong, C. Kim, T.G. Park, et al., High-strength carbon nanotube fibers fabricated by infiltration and curing of mussel-inspired catecholamine polymer, Adv. Mater. 23 (2011) 1971–1975.
[15] S. Ryu, J.B. Chou, K. Lee, D. Lee, S.H. Hong, R. Zhao, et al., Direct insulation-to-conduction transformation of adhesive catecholamine for simultaneous increases of electrical conductivity and mechanical strength of cnt fibers, Adv. Mater. 27 (2015) 3250–3255.
[16] Y.O. Im, S.H. Lee, T. Kim, J. Park, J. Lee, K.H. Lee, Utilization of carboxylic functional groups generated duringpurification of carbon nanotube fiber for its strength improvement, Appl. Surf. Sci. 392 (2017) 342–349.
[17] X. Lu, N. Hiremath, K. Hong, M.C. Evora, V.H. Ranson, A.K. Naskar, et al., Improving mechanical properties of carbon nanotube fibers through simultaneous solid-state cycloaddition and crosslinking, Nanotechnology 28 (2017) 145603.
[18] O.K. Park, W. Lee, J.Y. Hwang, N.H. You, Y. Jeong, S.M. Kim, et al., Mechanical and electrical properties of thermochemically cross-linked polymer carbon nanotube fibers, Composites Part A: Appl. S. 91 (2016) 222–228.
[19] O.K. Park, H. Choi, H. Jeong, Y. Jung, J. Yu, J.K. Lee, et al., High-modulus and strength carbon nanotube fibers using molecular cross-linking, Carbon 118 (2017) 413–421.
[20] E. Katz, Application of bifunctional reagents for immobilization of proteins on a carbon electrode surface: oriented immobilization of photosynthetic reaction centers, J. Electroanal. Chem. 365 (1994) 157–164.
[21] S. Wang, X. Wang, S.P. Jiang, PtRu nanoparticles supported on 1-aminopyrene-functionalized multiwalled carbon nanotubes and their electrocatalytic activity for methanol oxidation, Langmuir 24 (2008) 10505–10512.
[22] Y.Y. Zhang, J.S. Peng, M.Z. Li, E. Saiz, S.E. Wolf, Q.F. Cheng, Bioinspired supertough graphene fiber through sequential interfacial interactions, ACS Nano 12 (2017) 8901–8908.
[23] X. Zhang, Q. Li, Y. Tu, Y. Li, J.Y. Coulter, L. Zheng, et al., Strong carbon-nanotube fibers spun from long carbon-nanotube arrays, Small 3 (2007) 244–248.
[24] J. Foroughi, G.M. Spinks, S.R. Ghorbani, M.E. Kozlov, F. Safaei, G. Peleckis, et al., Preparation and characterization of hybrid conducting polymer–carbon nanotube yarn, Nanoscale 4 (2012) 940–945.
[25] C.H. Kwon, S.H. Lee, Y.B. Choi, J.A. Lee, S.H. Kim, H.H. Kim, et al., High-power biofuel cell textiles from woven biscrolled carbon nanotube yarns, Nat. Commun. 5 (2014) 3928.
[26] W. Guo, C. Liu, X. Sun, Z. Yang, H.G. Kia, H. Peng, Aligned carbon nanotube/polymer composite fibers with improved mechanical strength and electrical conductivity, J. Mater. Chem. 22 (2012) 903–908.
[27] H.J. Cho, H.M. Lee, E.G. OH, S.H. Lee, J.B. Park, H.J. Park, S.B. Yoon, C.H. Lee, G.H. Kwak, W.J. Lee, J.H. Kim, J.E. Kim, K.H. Lee, Hierarchical structure of carbon nanotube fibers, and the change of structure during densification by wet stretching, Carbon 136 (2018) 409–416.
[28] S.L. Zhang, A.Y. Hao, N. Nguyen, A. Oluwalowo, Z. Liu, Y. Dessureault, J.G. Park, R. Liang, Carbon nanotube/carbon composite fiber with improved strength and electrical conductivity via interface engineering, Carbon 144 (2019) 628–638.
[29] S.J. Wan, J.S. Peng, Y.C. Li, H. Hu, L. Jiang, Q.F. Cheng, Use of synergistic interactions to fabricate strong, tough, and conductive artificial nacre based on graphene oxide and chitosan, ACS Nano 9 (2015) 9830–9836.
[30] W. Cui, M.Z. Li, J.Y. Liu, B. Wang, C. Zhang, L. Jiang, et al., A strong integrated

strength and toughness artificial nacre based on dopamine cross-linked graphene oxide, ACS Nano 8 (2014) 9511–9517.
[31] H.W. Zhu, C.L. Xu, D.H. Wu, B.Q. Wei, R. Vajtai, P.M. Ajayan, Direct synthesis of long single-walled carbon nanotube strands, Science 296 (2002) 884–886.
[32] R. Meredith, 10-The tensile behaviour of raw cotton and other textile fibres, J. Text. I. Transactions 36 (1945) 107–130.
[33] J. Di, S. Fang, F.A. Moura, D.S. Galvao, J. Bykova, A. Aliev, et al., Strong, twist-stable carbon nanotube yarns and muscles by tension annealing at extreme temperatures, Adv. Mater. 28 (2016) 6598–6605.
[34] F.X. Kromm, T. Lorriot, B. Coutand, R. Harry, J.M. Quenisset, Tensile and creep properties of ultra high molecular weight PE fibres, Polym. Test. 22 (2003) 463–470.
[35] J.P. Rath, T.K. Chaki, D. Khastgir, Change in fiber properties due to the heat treatment of nylon 6 tire cords, J. Appl. Polym. Sci. 108 (2008) 3960–3967.
[36] F. Vollrath, D.P. Knight, Liquid crystalline spinning of spider silk, Nature 410 (2001) 541–548.
[37] C.A. Wang, Y. Huang, Q.F. Zan, H. Guo, S.Y. Cai, Biomimetic structure design — a possible approach to change the brittleness of ceramics in nature, Mater. Sci. Eng. C 11 (2000) 9–12.
[38] M. Motta, A. Moisala, I.A. Kinloch, A.H. Windle, High performance fibres from 'dog bone' carbon nanotubes, Adv. Mater. 19 (2007) 3721–3726.
[39] M. Naraghi, T. Filleter, A. Moravsky, M. Locascio, R.O. Loutfy, H.D. Espinosa, A multiscale study of high performance double-walled nanotube-polymer fibers, ACS Nano 4 (2010) 6463–6476.
[40] S. Gotovac, H. Honda, Y. Hattori, K. Takahashi, H. Kanoh, K. Kaneko, Effect of nanoscale curvature of single-walled carbon nanotubes on adsorption of polycyclic aromatic hydrocarbons, Nano Lett. 7 (2007) 583–587.
[41] L.M. Woods, Ş.C. Bădescu, T.L. Reinecke, Adsorption of simple benzene derivatives on carbon nanotubes, Phys. Rev. B 75 (2007) 155415.
[42] D.H. Lin, B.S. Xing, Adsorption of phenolic compounds by carbon nanotubes: role of aromaticity and substitution of hydroxyl groups, Environ. Sci. Technol. 42 (2008) 7254–7259.
[43] H. Ni, F.Y. Xu, A.P. Tomsia, E. Saiz, L. Jiang, Q.F. Cheng, Robust bioinspired graphene film via π-π cross-linking, ACS Appl. Mater. Interfaces 9 (2017) 24987–24992.